

1 **Anodic oxidation of sulfamethoxazole paired to cathodic hydrogen**  
2 **peroxide production**

3 Izba Ali<sup>1,2</sup>, Allisson Barros de Souza<sup>3</sup>, Steven De Laet<sup>1</sup>, Kwinten Van Eyck<sup>1</sup>, Raf Dewil<sup>2,4\*</sup>

4 <sup>1</sup> InOpSys - Mobiele waterzuivering voor chemie en farma, Zandvoortstraat 12a, 2800  
5 Mechelen, Belgium

6 <sup>2</sup> KU Leuven, Department of Chemical Engineering, Process and Environmental Technology  
7 Lab, Sint-Katelijne-Waver, Belgium

8 <sup>3</sup> Agilent Technologies, R&D and Marketing GmbH & Co. KG, Waldbronn, Germany

9 <sup>4</sup> University of Oxford, Department of Engineering Science, Parks Road, Oxford OX1 3PJ,  
10 United Kingdom

11 \* Corresponding author: [raf.dewil@kuleuven.be](mailto:raf.dewil@kuleuven.be)

## 12 **Abstract**

13 A double chamber electrochemical system is developed consisting of a boron-doped diamond  
14 (BDD) anode and a graphite cathode, which not only degrades sulfamethoxazole (SMX) but also  
15 simultaneously generates hydrogen peroxide ( $\text{H}_2\text{O}_2$ ). The degradation of degradation of SMX is  
16 carried out by (in)direct oxidation at the BDD anode and  $\text{H}_2\text{O}_2$  is produced by two electron oxygen  
17 ( $\text{O}_2$ ) reduction reaction (ORR) at the cathode. The effect of different parameters on the kinetics of  
18 both mechanisms was investigated. The performance of the system at the optimized conditions  
19 (pH 3, 0.05 M  $\text{Na}_2\text{SO}_4$  as electrolyte, and 10 mA as applied current) showed that after 180 min of  
20 electrolysis, SMX was almost all degraded (95% removal and ~90% COD reduction) as well as  
21 about 535  $\mu\text{M}$   $\text{H}_2\text{O}_2$  was accumulated. With the help LC-MS, five intermediates formed during  
22 SMX electrolysis were properly identified and a degradation pathway was proposed. This study  
23 advocate methods for improving the effectiveness of energy use in advanced wastewater treatment.

24 **Keywords** – Electrochemical advanced oxidation processes, sulfamethoxazole, hydrogen  
25 peroxide, boron-doped diamond, graphite, oxygen reduction reaction

## 26 **1. Introduction**

27 The frequent use of antibiotics and the inefficiency of conventional wastewater treatment plants to  
28 completely remove these compounds lead to their accumulation in natural water bodies (Meffe  
29 and de Bustamante, 2014; Tröger, et al., 2021). The presence of antibiotics in water bodies  
30 threatens human health by inducing antibiotic resistance. Therefore, there is an urgent need to  
31 implement tertiary (advanced) treatment technologies to ensure the removal of such compounds  
32 before their discharge into natural water bodies. In the present study, sulfamethoxazole (SMX), a  
33 typical sulfonamide antibiotic, was selected as a model pollutant due to its (i) frequent detection  
34 in the aquatic environment (Liu et al., 2017; Khasawneh and Palaniandy, 2021), (ii) recalcitrant

35 nature toward biological treatment (Prasannamedha and Kumar, 2020; Pariente et al., 2022), and  
36 (iii) inclusion in the Watch List of 2020/1161/EU (European Commission, 2020).

37 Recently, electrochemical advanced oxidation processes (eAOPs) have gained increasing attention  
38 due to their high efficiency and environmental compatibility (Nabgan et al., 2022). Boron-doped  
39 diamond (BDD) has been recognized as one of the best anode materials for the oxidation of organic  
40 pollutants due to its high overpotential for water hydrolysis, which facilitates the efficient  
41 production of hydroxyl radicals ( $\cdot\text{OH}$ ) (Marselli et al., 2003). BDD has also shown excellent  
42 stability toward corrosion resistance in extreme process conditions (Zhu et al., 2008).  
43 Traditionally, pollutant degradation in an eAOP is mainly caused by the (in)direct oxidation at the  
44 anode, coupled with  $\text{H}_2$  evolution at the cathode (Barrera-Díaz et al., 2014; Garcia-Segura et al.,  
45 2020). This  $\text{H}_2$  production is unfavorable for achieving a high energy efficiency since it does not  
46 contribute to pollutant oxidation and may lead to foaming issues. Therefore, there has been an  
47 increased interest in inducing the in-situ production of  $\text{H}_2\text{O}_2$  at the cathode by the  $2\text{e}^-$  ORR (Eq.  
48 1) (Ali et al., 2022). The detailed mechanism of  $\text{H}_2\text{O}_2$  production via ORR is reported in the  
49 literature (Wang et al., 2021b; Calle-Vallejo et al., 2013). Upon activation (e.g., by UV),  $\text{H}_2\text{O}_2$   
50 forms  $\cdot\text{OH}$ , which can degrade organic impurities in the water (Srivastav et al., 2019). The in-situ  
51 production of  $\text{H}_2\text{O}_2$  could thus offer numerous benefits over conventional eAOPs, including higher  
52 energy efficiency, enhanced oxidation of pollutants, and avoiding challenges associated with the  
53 transport, handling, and storage of  $\text{H}_2\text{O}_2$  (Qu and Liang, 2022; Wang et al., 2021a). Literature  
54 suggests that carbonaceous materials such as graphite, graphene and carbon nanotubes are suitable  
55 for cathodic  $\text{H}_2\text{O}_2$  production due to the presence of intrinsic defects, e.g., holes, positive  
56 topological disclinations, and  $\text{sp}^3$ -C sites, which act as active sites for the formation of ORR  
57 intermediates (Marselli et al., 2003; Zhang et al., 2020). Among these, graphite has been selected

58 due to its stability against pressure, temperature, and chemicals as well as its very low cost  
 59 compared to other materials (Lee et al., 2008).



60 Although, few studies have reported electrochemical degradation of SMX using BDD anode  
 61 (Table 1), however they lack to demonstrate the possibility of co-generating  $\text{H}_2\text{O}_2$  in the same  
 62 system. For instance, Hai et al. (2020) systematically investigated SMX oxidation but fell short of  
 63 demonstrating concurrent  $\text{H}_2\text{O}_2$  production. In the light of this, we proposed to enhance the energy  
 64 efficiency of the electrochemical system by instigating in-situ generation of  $\text{H}_2\text{O}_2$ . Herein, we  
 65 investigate the effect of various process parameters on the  $\text{H}_2\text{O}_2$  production at cathode and  
 66 oxidation of SMX at anode. The cathodic and anodic processes were individually assessed by  
 67 using a cation exchange membrane in the reactor, which separates the catholyte and the anolyte.  
 68 Prior to looking at SMX degradation, the impact of parameters on  $\text{H}_2\text{O}_2$  production was examined.  
 69 After determining the effect of the selected parameters on both (cathodic and anodic) processes,  
 70 optimal conditions were assessed for efficient outputs at both sides of the cell. Furthermore, a  
 71 degradation pathway was proposed and transformation products (TPs) of SMX electrolysis were  
 72 also identified.

73 Table 1. Performance comparison of published literature SMX degradation using BDD electrode

Experimental conditions					SMX removal		Reference
Cathode material	Anode material	[SMX] <sub>0</sub> , mg L <sup>-1</sup>	V/flow rate	Electrolyte	I/J	rate, efficiency and reaction time	
Stainless steel plates	BDD, 36 cm <sup>2</sup>	250	5 L min <sup>-1</sup>	0.05 M Na <sub>2</sub> CO <sub>3</sub>	36 mA cm <sup>-2</sup>	k = 0.0125 min <sup>-1</sup> ~99% in 180 min	(Amorim et al., 2013)

Zirconium, 69 cm <sup>2</sup>	BDD, 69 cm <sup>2</sup>	15	1 L	0.02 M K <sub>2</sub> SO <sub>4</sub>	7.2 mA cm <sup>-2</sup>	k = 0.0168 min <sup>-1</sup> 99% in 300 min	(Lan et al., 2017)
BDD	BDD, 189 cm <sup>2</sup>	0.5	500 L h <sup>-1</sup>		900 mA	k = 0.0054 min <sup>-1</sup> >60% in 180 min	(Loos et al., 2018)
Stainless steel, 2 cm <sup>2</sup>	BDD, 2 cm <sup>2</sup>	30	350 mL	0.1 M Na <sub>2</sub> SO <sub>4</sub>	30 mA	k = 0.02 min <sup>-1</sup> ~97% in 180 min	(Hai et al., 2020)
Pt	TiO <sub>2</sub> - BDD	50	50 mL	0.05 M phospha te buffer	75 mA	~92% in 180 min	(Suzuki et al., 2022)

74 I = applied current, J = applied current density, V = volume, [SMX]<sub>0</sub> = initial SMX concentration, k = rate constant.

## 75 2. Materials and methods

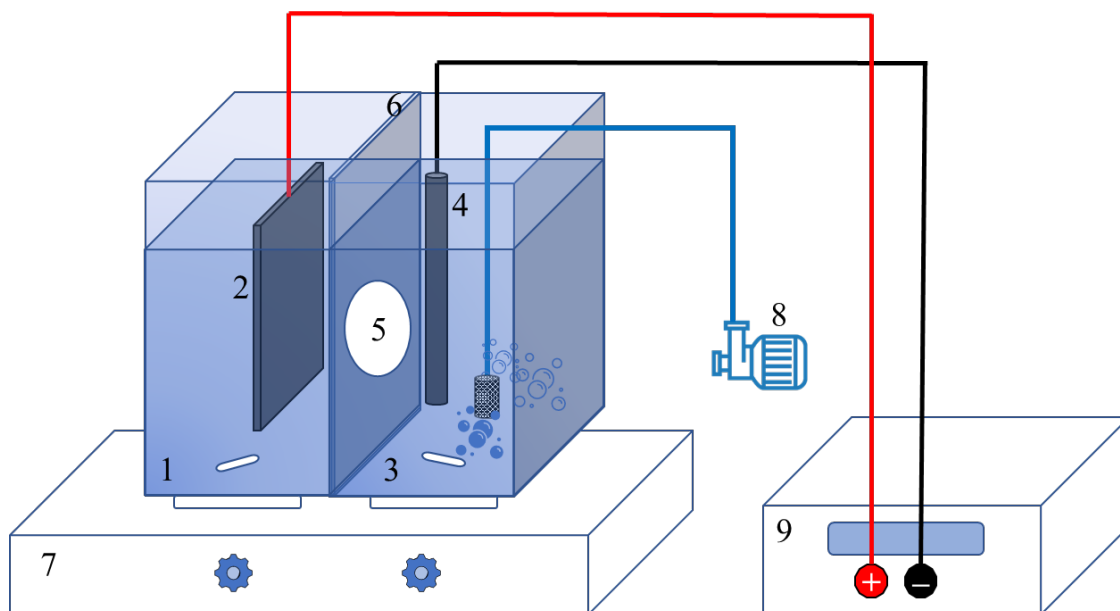
### 76 2.1. Chemicals and materials

77 Analytical standard SMX (≥98.0%), hydrogen peroxide (H<sub>2</sub>O<sub>2</sub>, 30% (w/w)), sulfuric acid (H<sub>2</sub>SO<sub>4</sub>,  
78 ≥95%), sodium sulfate (Na<sub>2</sub>SO<sub>4</sub>, ≥99%) were purchased from Sigma–Aldrich (Overijse, Belgium).  
79 HPLC grade acetonitrile (ACN, ≥99.8%) and formic acid (FA, ≥99%) were purchased from VRW  
80 (Darmstadt, Germany). BDD plates were supplied by NeoCoat (La Chaux-de-Fonds, Switzerland)  
81 and graphite rod electrodes were supplied by Thermo Fisher Scientific (Karlsruhe, Germany).  
82 They were used as anode and cathode respectively. Nafion 117 membrane and Ag/AgCl reference  
83 electrode was purchased from redox.me (Norrköping, Sweden).

### 84 2.2. Experimental setup

85 A schematic overview of the double chamber electrochemical reactor used in this study is  
86 presented in Fig. 1. The cell was constructed of 0.6 cm thick polyvinyl chloride (PVC) and  
87 consisted of two separate chambers connected by a circular window (6 cm diameter) at the center  
88 of the PVC plate separating both chambers. Each chamber has a working volume of 400 mL (15

89 cm high, 7 cm long and 7 cm wide). The reactor's dimensions were chosen so that the electrodes  
90 could be readily contained and each chamber had a working volume of 400 mL, which is primarily  
91 reported in the literature for similar experiments. In the window, a cation exchange membrane  
92 (Nafion 117) was sandwiched between 0.3 cm thick two polytetrafluoroethylene (PTFE) gaskets.  
93 The membrane separates the anolyte and catholyte. Before the start of an experiment, the  
94 membrane was activated following the procedure described in the supporting information (Text  
95 S1). Additionally, the tendency of the membrane toward SMX adsorption was examined and found  
96 to be negligible. A constant current was applied by means of an Autolab PGSTAT302N  
97 potentiostat, obtained from Metrohm (Antwerpen, Belgium). The electrochemical oxidation of  
98 SMX occurred at the BDD electrode in the anodic chamber, whereas H<sub>2</sub>O<sub>2</sub> generation was attained  
99 at the graphite electrode in the cathodic chamber. Air was continuously bubbled into the cathodic  
100 compartment with the help of an aerator, consisting of a single air injection nozzle connected to a  
101 diffuser.



102

103 Fig. 1. The experimental setup used in the study: 1. Anodic chamber, 2. BDD plate electrode, 3. Cathodic chamber,  
104 4. Graphite rod electrode, 5. Cation exchange membrane, 6. PTFE gaskets, 7. Stirring plate, 8. Aeration pump and 9.  
105 Potentiostat

106 For preparation of experimental solutions, chemicals were dissolved in ultra-pure (Milli-Q) water.  
107 For complete dissolution of SMX in the anolyte, 2 h of mixing on a stirring plate was found to be  
108 sufficient. All experiments were performed in triplicate for 180 min.

### 109 2.3. Analytical techniques

110 The production of  $H_2O_2$  in the catholyte was analyzed by using titanium(IV) oxalate as explained  
111 in the supporting information (Text S2 and Fig. S1). A portable spectrophotometer (HACH  
112 DR1900, Nazareth, BE) was used for spectrophotometric and COD measurements.

113 The removal of SMX in the anolyte was tracked with an Agilent 1260 Infinity II Prime Online  
114 HPLC System (Agilent Technologies, Waldbronn, Germany). The system was equipped with a  
115 binary pump, DAD detector, and an isocratic pump; the HPLC system enables real-time SMX  
116 monitoring via direct injections from the reactor onto the column at scheduled time intervals and

117 retain-sample features, which draws samples from the reactor into HPLC vials for additional  
118 offline LC/MS analysis. For HPLC separation, an EC-C18 column (Poroshell 120, 2.1 x 50 mm;  
119 particle size ( $d_p$ ) 1.9  $\mu\text{m}$ ) was used. The mobile phase was a combination of (A) 0.1% FA in water  
120 and (B) 0.1% FA in ACN. The elution method consisted of a gradient increasing from 5% to 95%  
121 B over 5 min, maintained at 95% for 1 min, quickly returned to 5% B (i.e., initial condition) and  
122 maintained there for the next 0.5 min for re-equilibration of the column. The flow rate was set at  
123 0.5 mL/min, and SMX UV absorbance detection was performed at 270 nm. To meticulously  
124 observe the degradation of SMX, two multilevel calibration curves were constructed at 6 levels  
125 for (i) higher concentrations ranging between 0.5–25  $\text{mg L}^{-1}$  and (ii) lower concentrations in the  
126 range of 0.025–1  $\text{mg L}^{-1}$ . Over the entire range of concentrations, linear calibration curves with  
127  $R^2 > 0.999$  were obtained. The injection volumes were 3  $\mu\text{L}$  and 5  $\mu\text{L}$  for higher and lower  
128 concentrations, respectively.

129 The SMX TPs were identified using UHPLC-QTOF-MS. An Agilent 1290 Infinity II UHPLC  
130 system (Agilent Technologies) equipped with a binary pump, an autosampler, a column  
131 thermostat, and a diode array detector (DAD) was used in combination with an Agilent 6550  
132 iFunnel quadrupole-time-of-flight mass spectrometer (Q-TOF MS). The column used to carry out  
133 separations was a Zorbax SB-Aq RRHD (2.1  $\times$  100 mm;  $d_p$  1.8  $\mu\text{m}$ ; Agilent, USA). The mobile  
134 phase composition was similar to the HPLC-UV analysis; however, the LC method was slightly  
135 adapted for the UHPLC–MS analysis. The method included a gradient increasing from 5% to 95%  
136 B in 7 min, then it was held at the same condition for 1 min, then B was reduced back to 5% in 0.1  
137 min and held for 1 min for re-equilibration. The mobile phase flow rate was 0.4 mL/min, the  
138 injection volume was 2  $\mu\text{L}$ , and DAD UV-absorbance detection was performed at 270 nm. The Q-  
139 TOF MS was operated in the 2 GHz Extended Dynamic Range mode. The ionization was



140 performed in positive electrospray ionization mode using Dual Agilent Jet Stream Technology  
141 operated at a gas temperature of 230 °C, drying gas flow of 13 L/min, nebulizer pressure of 35 psi  
142 and a sheath gas temperature and flow of 350 °C and 12 L/min, respectively. The capillary voltage  
143 was set at 4000 V, nozzle voltage at 500 V and fragmentor at 350 V. MS and MS/MS spectra were  
144 collected at 4 spectra/s. The data analysis was performed using Agilent MassHunter Qualitative  
145 software (version 10.0), Profinder (version 10.0), and Mass Profiler Professional (version 15.1).

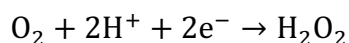
### 146 **3. Results and discussion**

#### 147 **3.1. Cathodic process optimization for H<sub>2</sub>O<sub>2</sub> production**

148 Usually, the key parameters which influence H<sub>2</sub>O<sub>2</sub> production efficiency at the cathode involve  
149 pH, concentration of the electrolyte and applied current (Pang et al., 2020; Xue et al., 2021).  
150 Therefore, the effect of these parameters to determine the optimal conditions is investigated and  
151 discussed below.

##### 152 **3.1.1. Effect of pH**

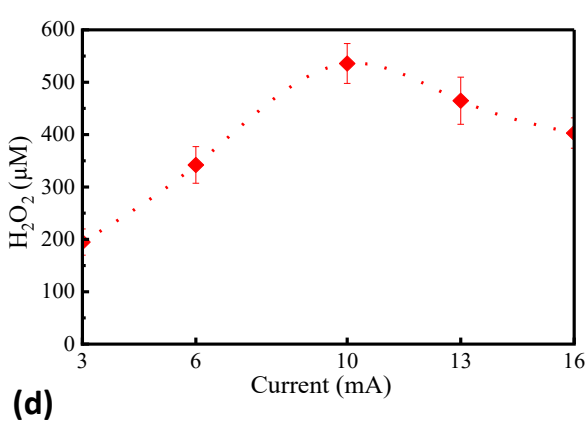
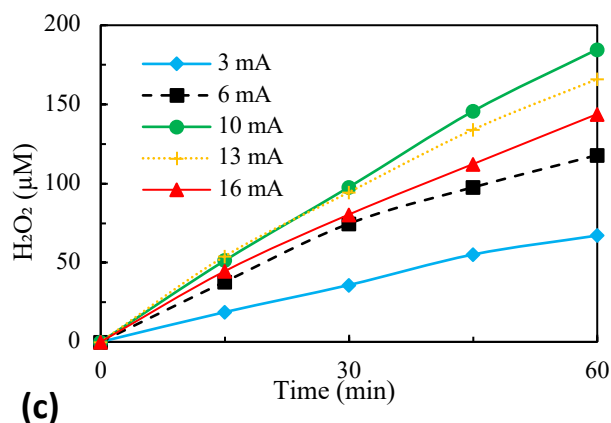
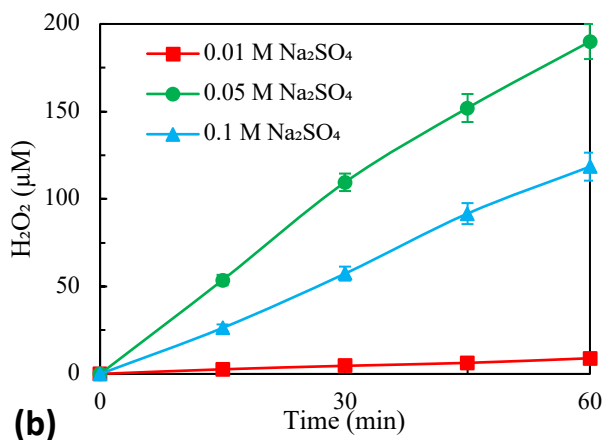
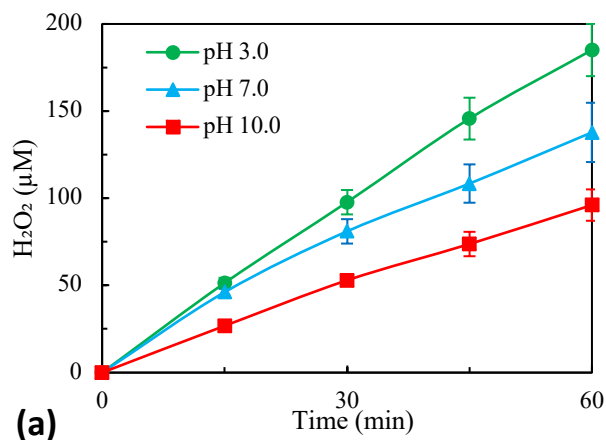
153 Fig. 2a shows the effect of pH on the accumulated concentration of H<sub>2</sub>O<sub>2</sub>. It was observed that pH  
154 3.0 was the most favorable for the production of H<sub>2</sub>O<sub>2</sub>. This can be understood from the reaction  
155 Eq. 2, which implies that the presence of H<sup>+</sup> is required for O<sub>2</sub> reduction to form H<sub>2</sub>O<sub>2</sub>. Therefore,  
156 electro-generation of H<sub>2</sub>O<sub>2</sub> decreased (185, 137 and 90 μM) as the pH was increased (3.0, 7.0 and  
157 10.0, respectively). These results are also in agreement with previously reported findings for  
158 graphite electrode material (Peralta et al., 2013). Additionally, H<sub>2</sub>O<sub>2</sub> is unstable in alkaline  
159 solutions and, therefore may self-decompose to O<sub>2</sub> and H<sub>2</sub>O (Lu et al., 2018). Based on this, pH  
160 3.0 was selected for the catholyte in further experiments.



2

### 161 3.1.2. Effect of electrolyte concentration

162 In an electrochemical process, the conductivity of the electrolyte solution increases with the  
163 increase in the amount of added salt. Thus, to ensure good ion transferability (i.e., higher  
164 conductivity) in the aqueous medium, the electrolyte concentration should be higher (Zhou et al.,  
165 2019). Fig. 2b shows the effect of electrolyte ( $\text{Na}_2\text{SO}_4$ ) concentration, added at a concentration of  
166 0.01 M, 0.05 M, and 0.1 M. At the lowest concentration (0.01 M  $\text{Na}_2\text{SO}_4$ ) almost no  $\text{H}_2\text{O}_2$   
167 production was observed, this could be due to a too low amount of supporting electrolyte ions (i.e.,  
168 low conductivity). The optimal electrolyte concentration was found to be 0.05 M  $\text{Na}_2\text{SO}_4$ . Whereas  
169 the decrease in  $\text{H}_2\text{O}_2$  production at higher  $\text{Na}_2\text{SO}_4$  concentrations (0.1 M) could be assigned to the  
170 premise of salt particles attachment on the electrode surface, causing a reduction in the number of  
171 active sites or a change in the active site chemistry. This explanation was further supported by the  
172 results of scanning electron microscopy (SEM) surface elemental composition analysis, which  
173 showed the presence of relatively high amount of Na and S atoms on the electrode surface in 0.1  
174 M as compared to 0.05 M or 0.01 M  $\text{Na}_2\text{SO}_4$ , respectively (Fig. S2). These findings are also in  
175 line with the previously published literature (Qiang et al., 2002; Tian et al., 2020). Moreover, it  
176 was also verified during the anodic process optimization (Section 3.2.2), that higher salt  
177 concentrations lead to a decrease in the desired reaction rate. Therefore, 0.05 M  $\text{Na}_2\text{SO}_4$  electrolyte  
178 concentration was opted as optimal.



179

180

181 Fig. 2. Effect of (a) pH, (b) electrolyte concentration, (c) applied current on H<sub>2</sub>O<sub>2</sub> production in the cathodic  
 182 compartment, and (d) H<sub>2</sub>O<sub>2</sub> accumulation after 180 min. Other conditions: pH = 3.0, [Na<sub>2</sub>SO<sub>4</sub>] = 0.05 M, applied  
 183 current = 10 mA

### 184 3.1.3. Effect of applied current

185 The effect of the applied current on the electrochemical generation of H<sub>2</sub>O<sub>2</sub> at the graphite cathode  
 186 is given in Fig. 2c and d. The results outside the tested range were not significant i.e., H<sub>2</sub>O<sub>2</sub>  
 187 concentration was lower than the detection limit. At any applied current, the concentration of H<sub>2</sub>O<sub>2</sub>  
 188 was found to be continuously accumulating due to the separation of the chambers, since this avoids  
 189 the autooxidation of H<sub>2</sub>O<sub>2</sub> at the anode surface (Li et al., 2021). The highest H<sub>2</sub>O<sub>2</sub> yield was  
 190 obtained at 10 mA and a shift from the optimal current resulted in a noticeable decrease in the

191 H<sub>2</sub>O<sub>2</sub> production. This indicates that the H<sub>2</sub>O<sub>2</sub> formation reaction is dependent on the applied  
192 current (Pozzo et al., 2005). The reason is that at higher current values, 4e<sup>-</sup> reduction of O<sub>2</sub> (Eq.  
193 3) starts to compete with the 2e<sup>-</sup> ORR (Eq. 2).



194 From the results obtained in sections 3.1.1 – 3.1.3, it can be inferred that at an applied current of  
195 10 mA and a 0.05 M Na<sub>2</sub>SO<sub>4</sub> concentration at pH 3.0, the most efficient H<sub>2</sub>O<sub>2</sub> production is  
196 achieved (Fig. 2d). Thus, after determining the optimal parameters for cathodic process (i.e., H<sub>2</sub>O<sub>2</sub>  
197 production), in the next steps the optimal conditions for anodic process (i.e., SMX degradation)  
198 were analyzed, while simultaneously monitoring their impact on H<sub>2</sub>O<sub>2</sub> production.

### 199 **3.2. Anodic process optimization for SMX degradation**

200 During anodic process optimization for SMX degradation, the initial pH and electrolyte  
201 concentration in the cathodic chamber were kept at 3.0 and 0.05 M Na<sub>2</sub>SO<sub>4</sub>, respectively. Based  
202 on the available published data, three of the most relevant parameters (initial pH, initial SMX  
203 concentration, and applied current) were selected to determine their influence on SMX degradation  
204 concurrently monitoring H<sub>2</sub>O<sub>2</sub> production.

#### 205 **3.2.1. Process kinetics**

206 The oxidation of SMX at the BDD anode, for instance through its reaction with hydroxyl radicals  
207 (·OH), is what causes its degradation. However, in all experiments, pseudo-first order kinetics for  
208 SMX oxidation were confirmed since a straight line with R<sup>2</sup> > 0.99 was obtained by plotting ln  
209 ([SMX]/[SMX]<sub>0</sub>) as a function of time (Eq. 4). This indicates that the SMX degradation was not  
210 limited by the amount of hydroxyl radicals generated by the anode. The degradation kinetics can,  
211 therefore, be described as pseudo first order.

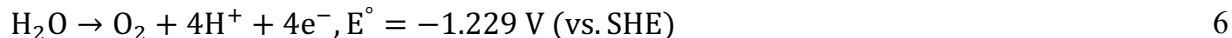
$$\ln \left( \frac{[\text{SMX}]}{[\text{SMX}]_0} \right) = k \times t \quad 4$$

212 where  $[\text{SMX}]_0$  is initial SMX conc. ( $\text{mg L}^{-1}$ ),  $[\text{SMX}]$  is the conc. of SMX at any time, and  $t$  is time  
213 (min). The slope in the equation is negative and represents the pseudo-first order degradation rate  
214 constant  $k$  ( $\text{min}^{-1}$ ).

### 215 **3.2.2. Effect of initial pH**

216 The effect of the initial pH on SMX degradation was investigated at pH values of 2.0, 7.0, and  
217 12.0. However, during an electrochemical process, the redox reactions change the pH in both  
218 compartments (Obata et al., 2020). The oxidation reaction taking place at the anode decreases the  
219 pH, whereas the reduction taking place at the cathode causes an increase in pH. Therefore, to  
220 properly understand the effect of pH, the experiments were first carried out at constant pH (7.0),  
221 by adding buffer to keep it from changing over the course of experiment. For this, phosphate buffer  
222 solutions (PBS) at different concentrations (0.001, 0.01, and 0.1 M) were employed. The higher  
223 the buffer concentration, the better the tendency to maintain the pH at the required value, which  
224 was also reflected by end pH of the experiment. For instance, the final pH in the anodic  
225 compartment was 3.0, 5.7, and 6.9 for 0.001, 0.01, and 0.1 M PBS concentration, respectively.  
226 Nonetheless, the addition of phosphate salts to provide a pH buffer has a negative effect on SMX  
227 degradation. As shown in Fig. 3a, increasing the amounts of buffering salts decreases the  
228 degradation kinetics and there are several reasons to explain this behavior (Sifuna et al., 2016).  
229 According to the literature, increasing salt concentration increase the conductivity of the solution,  
230 but when the concentration exceeds a specific threshold, a salt film may be formed on the electrode  
231 surface, reducing the number of active sites on the electrode. The active sites are the places where  
232 pollutants bind at the anode surface and oxidize by (i) direct oxidation (direct charge transfer

233 between the pollutant and anode surface) or (ii) indirect oxidation (oxidation due to in situ  
234 generation of reactive oxygen species at the anode [Eq. 5]) (Ganiyu et al., 2021). Therefore, the  
235 salt film covering the active sites leads to a decrease in the pollutant degradation rate (Cho and  
236 Kim, 2020). Furthermore, to maintain the pH at a constant level, the buffer system captures the  
237 excessive number of protons produced by the oxidation reactions at the anode (Eq. 6). As a result,  
238 the H<sub>2</sub>O<sub>2</sub> production in the cathodic compartment could also be lowered. This was further  
239 confirmed by performing an experiment (with and without buffer) (Fig. 3d). The H<sub>2</sub>O<sub>2</sub> production  
240 was substantially reduced to 100 μM (with buffer) compared to 535 μM (without buffer).  
241 Therefore, in the next experiment, the pH was set to the desired value only once at the start of the  
242 experiment and was not altered later during a full experimental run.



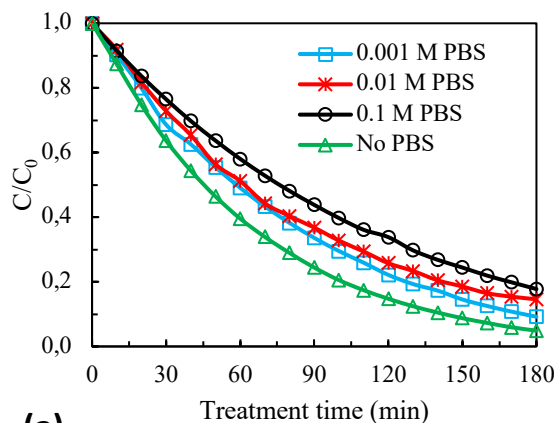
243 The influence of the initial pH on the degradation of SMX without the application of a buffer is  
244 depicted in Fig. 3b. After 180 min of electrolysis, 94%, 95%, and 63% SMX was removed at pH  
245 2.0, 7.0, and 12.0, respectively, showing that the SMX degradation is favored in the acidic to  
246 neutral pH range. This observation can be explained by the pK<sub>a</sub> values of SMX (pK<sub>a1</sub>=1.8 and  
247 pK<sub>a2</sub>=5.6) and its corresponding ionization structures (Fig. S3). At pH values lower than 1.8 or  
248 higher than 5.6, SMX exists primarily in its ionized form (cationic at lower pH and anionic at  
249 higher pH). However, for pH between 1.8 and 5.6, SMX is present predominantly in its molecular  
250 form (i.e., less charged), which reduces the intermolecular electrostatic repulsion and improves the  
251 mass transfer of SMX to the electrode surface (Lin et al., 2013; Milh et al., 2020).

### 252 3.2.3. Effect of the initial concentration of SMX

253 The effect of  $[\text{SMX}]_0$  is shown in Fig. 3c. The  $k$  values were 0.0249, 0.0168, and 0.0146  $\text{min}^{-1}$   
254 for  $[\text{SMX}]_0$  of 0.25, 12.5, and 25  $\text{mg L}^{-1}$ , respectively. As  $[\text{SMX}]_0$  increased from 0.25 to 25  
255  $\text{mg L}^{-1}$ , the removal rate almost halved, which suggests that the electrolysis of SMX is a diffusion  
256 control process (Dirany et al., 2010). In a diffusion control system, the electrochemical oxidation  
257 rate is higher than that of diffusion (Trinh, 2011). So, at lower initial concentrations, the  
258 electrocatalytic oxidation rate was greater than the diffusion of SMX; thus, SMX was oxidized  
259 effectively. This is because, at the same initial electrolyte concentration and applied current, the  
260 amount of  $\cdot\text{OH}$  produced is the same. However, when high pollutant concentration is applied, it  
261 increases the quantity of pollutants that react with these hydroxyl radicals as well as more  
262 intermediate products are formed, which further decreases the amount of hydroxyl radicals  
263 available per unit of pollutants (Feng et al., 2022).

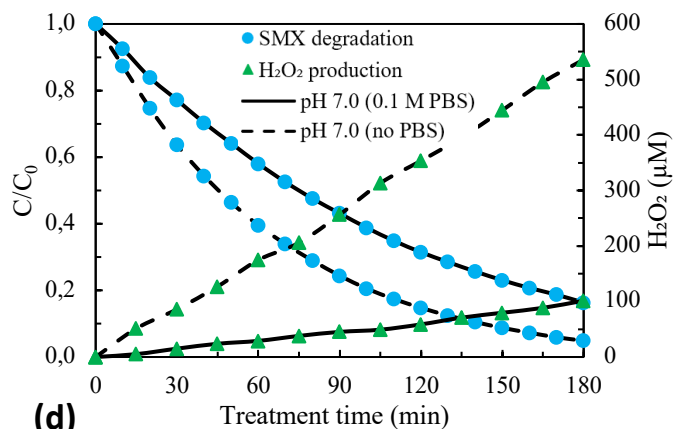
#### 264 **3.2.4. Effect of applied current**

265 As the electrodes are positioned in their respective chambers separated by a membrane, the  
266 electrolytes in both compartments cannot mix, which enables the attainment of different pH and  
267 electrolyte composition in each compartment. However, the applied current influences the  
268 reactions at both electrodes. Therefore, it is a critical parameter that can significantly affect the  
269 process efficiency at both sides of the reactor.

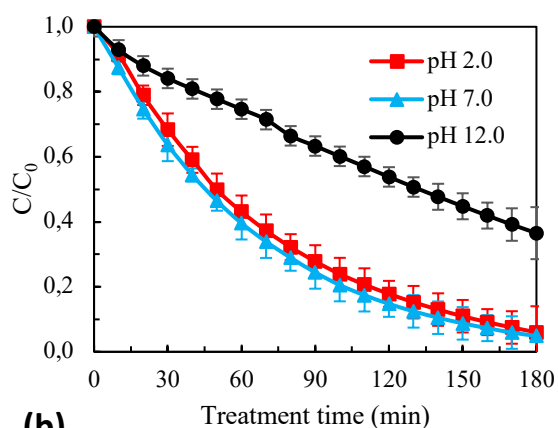


270

(a)

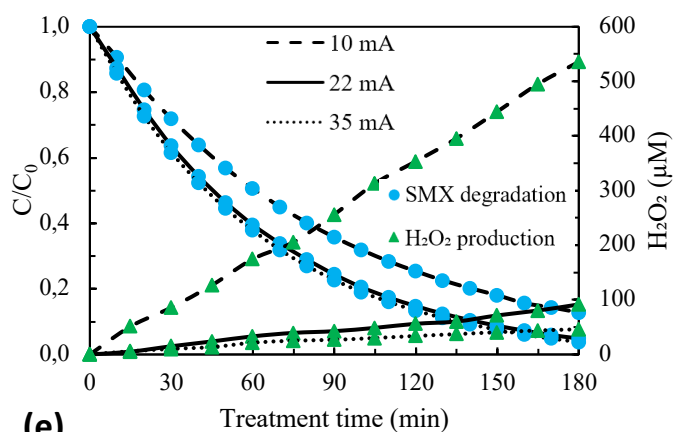


(d)

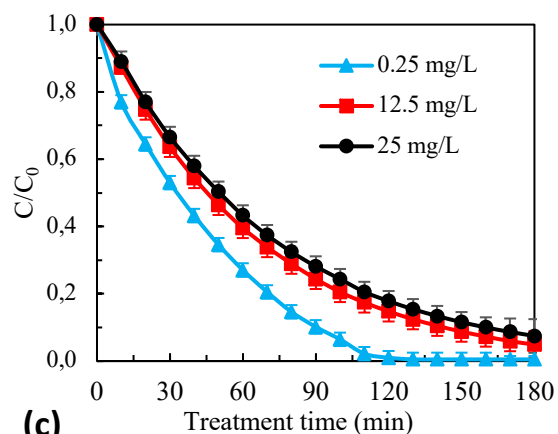


271

(b)

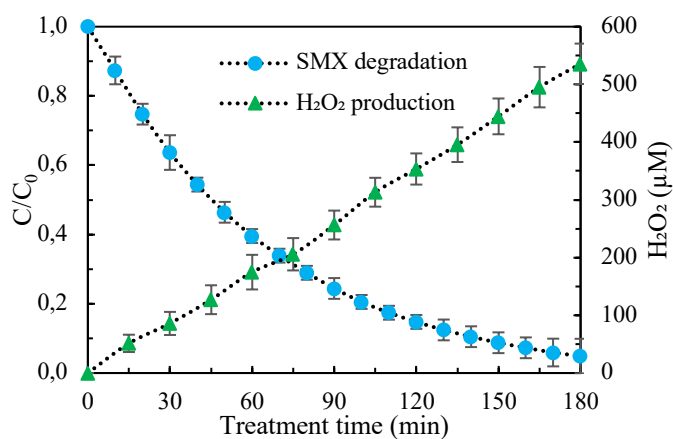


(e)



272

(c)



273 Fig. 3. Effect of (a) PBS concentrations on SMX removal, (b) initial pH, (c)  $[SMX]_0$ , (d) PBS vs SMX degradation  
 274 and  $H_2O_2$  production, (e) applied current values on the SMX degradation and  $H_2O_2$  production, and (f) optimized  
 275 conditions. Other conditions: applied current = 10 mA, pH = 7.0,  $[SMX]_0 = 12.5 \text{ mg L}^{-1}$ .

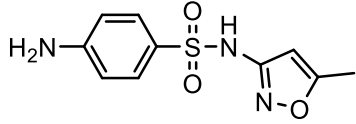
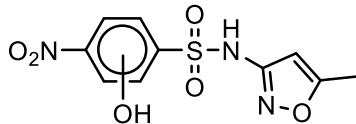
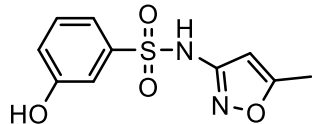
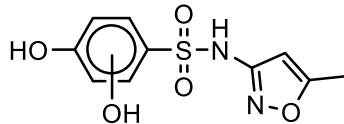
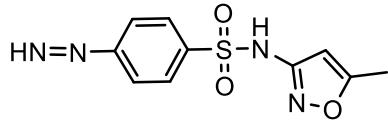
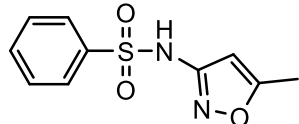


276 Fig. 3e shows that increase in applied current does not significantly improve the SMX removal.  
277 The k values were 0.0115, 0.0168, and 0.0178 min<sup>-1</sup>, when the applied current was 10, 22.5 and  
278 35 mA, whereas the removal efficiency was 87, 95, and 96%, respectively. An increase in the  
279 applied current value should increase the production of ·OH at the anode, and thus shall enhance  
280 the oxidation of SMX (Hai et al., 2020). This limited change in degradation efficiency can be  
281 attributed to O<sub>2</sub> evolution reaction, which increases with applied current, resulting in a decrease in  
282 the degradation efficiency (Wang et al., 2020; Fu et al., 2022). Additionally, as the oxidation of  
283 pollutant (SMX) at the anode surface is limited by the mass transfer kinetics, it restricts the  
284 diffusion of SMX molecules to the anode surface, thereby reducing the efficiency of excess current  
285 (Song et al., 2017). On the other hand, since production of H<sub>2</sub>O<sub>2</sub> is significantly influenced by the  
286 applied current, it diminishes in the cathodic compartment as a consequent of increasing current.  
287 Therefore, 10 mA can be inferred as the optimum current value to achieve the best results in both  
288 compartments.

### 289 **3.3. Identification of transformation products**

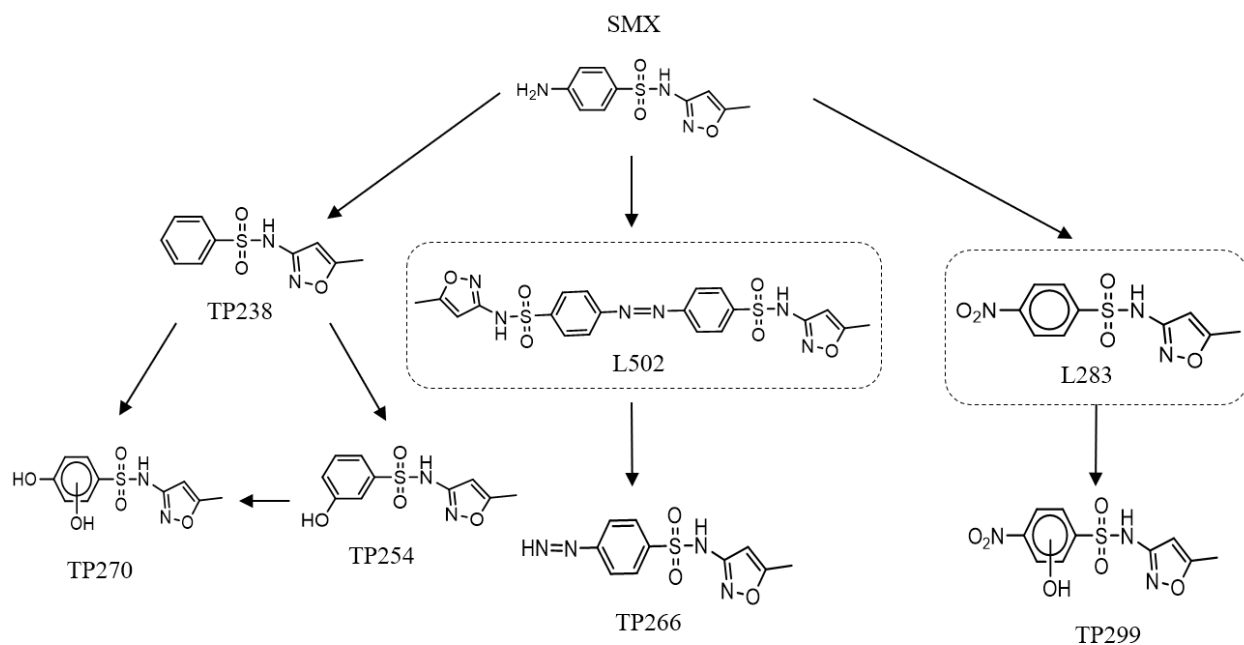
290 With the help of UHPLC-DAD-QTOF MS, five TPs formed during the electrolysis of SMX were  
291 identified. The TPs that were detected and confirmed by MS/MS are marked with TP. Other  
292 intermediates that have been suggested based on previous studies are marked with L and encircled  
293 in dotted rectangles. Fig. 4 depicts the proposed degradation pathway and Table 2 shows the  
294 identified TPs, along with their tentatively proposed structures based on their accurate masses,  
295 MS/MS fragmentation and literature data (Feng et al., 2022; Hai et al., 2020; Milh et al., 2021;  
296 Reddy and Subrahmanyam, 2015; Yang et al., 2017). The MS/MS fragmentation spectra of all TPs  
297 are provided in Fig. S4.

298 Table 2. The transformation products of SMX formed due to its electrochemical oxidation at the BDD anode

Name	Proposed elemental formula	Precursor $m/z$ ( $[M+H]^+$ )	Proposed molecular structure
SMX	$C_{10}H_{11}N_3O_3S$	254.0594	
TP299	$C_{10}H_9N_3O_6S$	300.0228	
TP254	$C_{10}H_{10}N_2O_4S$	255.0445	
TP270	$C_{10}H_{10}N_2O_5S$	271.0384	
TP266	$C_{10}H_{10}N_4O_3$	267.0537	
TP238	$C_{10}H_{10}N_2O_3S$	239.0484	

299 A TP299 with experimental  $m/z$  300.0288 was identified. TP299 was formed by the oxidation of  
 300 an aromatic amino group, creating a nitro group, its further hydroxylation on the aromatic ring  
 301 (Suzuki et al., 2022). The MS/MS fragments ( $m/z$  77.0368, 98.0467, 122.0194, 201.9749, and  
 302 205.0274) of TP299 and their tentative structures confirmed the presence of TP299. The analysis  
 303 of fragments revealed that the addition of the OH-group is most likely located on the benzene ring

304 and not on the isoxazole ring. TP299 was also previously identified in the literature as a TP of  
305 SMX during its oxidation at the BDD anode, which further validates its formation during the  
306 process (Hai et al., 2020; Rajab et al., 2013).



307

308 Fig. 4. A pathway proposed for degradation of SMX

309 TP266 (267.0539) and TP238 (239.0491) were detected, but these TPs were not previously  
310 reported in the literature. However, their MS/MS fragmentation confirmed their presence as per  
311 their elucidated structures. The MS/MS fragments of TP266 were observed with experimental  $m/z$   
312 106.0531, 108.0758, 77.0385, 161.0734, 172.0518, and TP238 with experimental  $m/z$  144.0454,  
313 140.9999, 77.0380, and 72.0444. Similarly, TP254 was found with the MS/MS fragments of  
314 93.0322, 99.0539, and 160.0358. It is resulted from the hydroxylation of TP238. The literature  
315 suggests that the *ipso*- addition of  $\cdot\text{OH}$  to the SMX structure and the removal of amino groups  
316 might result in the formation of TP254 (Radjenovic and Petrovic, 2017). Further hydroxylation of  
317 the aromatic ring in TP254 yields dihydroxylated product TP270 (271.0384). The MS/MS

318 fragments obtained by the fragmentation of TP270 have experimental  $m/z$  99.0536, 109.0281,  
319 163.0486, and 172.9889; thus, these were considered to be a conforming representative of TP270.  
320 It can be observed that most of the TPs identified in the present study were formed due to  $\cdot\text{OH}$   
321 attacking of SMX. Additionally, ECOSAR software was used to estimate the toxicity of TPs, and  
322 the results suggest that the TPs produced during the treatment are less harmful than the parent  
323 compound (Table S2). The evolution and relative abundance of the identified TPs with respect to  
324 treatment time are given in Fig. S5, which illustrates that most of the TPs had also been degraded  
325 during the treatment time. This demonstrates the system's capability to effectively treat the  
326 contaminant.

### 327 **3.4. Discussion**

328 A detailed description of all degradation experiments performed under different conditions can be  
329 found in Table S1, where high  $R^2$  values again affirm the pseudo-first order reaction kinetics. The  
330 effect of the selected parameters on the cathodic and anodic processes was examined individually,  
331 which was possible due to the use of cation exchange membrane since it can separate the catholyte  
332 from anolyte. The cell division enables to operate at a different pH and electrolyte concentration  
333 in each compartment. First the effect of changing the parameters in the cathodic chamber was  
334 analyzed and optimal conditions for the  $\text{H}_2\text{O}_2$  production were determined. Subsequently, the  
335 effect of the selected parameters in the anodic chamber was examined while adopting the pH and  
336 electrolyte concentration in cathodic compartment to its optimal values (pH 3.0 and 0.05 M  
337  $\text{Na}_2\text{SO}_4$ , respectively). According to the results of this study, it was observed that there is no  
338 significant difference in the optimal parameters of both compartments. For the initial pH values,  
339 the cathodic compartment yields an optimal efficiency at 3.0 and the anodic compartment yields  
340 an optimal efficiency at 3.0–7.0. An electrolyte concentration of 0.05 M  $\text{Na}_2\text{SO}_4$  was sufficient in

341 both compartments. The production of  $\text{H}_2\text{O}_2$  as well as SMX degradation were optimum at 10 mA  
342 and were not significantly improved at higher currents. Finally, the electrochemical system was  
343 operated at the optimized parameters (Fig. 3f), to achieve 95% SMX degradation (~90% COD  
344 removal) and approximately 535  $\mu\text{M}$   $\text{H}_2\text{O}_2$  in 180 min. The  $\text{H}_2\text{O}_2$  produced in this system can be  
345 activated (e.g., with UV or  $\text{Fe}^{+2}$ ) to accomplish a higher degradation efficiency. Moreover, these  
346 conditions could also be implemented in a single chamber configuration (i.e., without membrane  
347 separation) due to similarity in the optimal conditions of both compartments. Single chamber  
348 configuration could slightly lower the efficiency of the system (Fig. S6), but it is beneficial from  
349 an economic point of view for real-scale applications since it can avoid the need to install a  
350 membrane in the reactor. Overall, the optimized electrochemical system uses less energy and  
351 achieve significantly better outputs as compared to the previous studies (e.g., in Table 1). Thus,  
352 these results manifest that an integrated reactor functionality (which on the one hand degrades  
353 pollutant and on the other hand produces a powerful oxidizer i.e.,  $\text{H}_2\text{O}_2$ ) is realistic and offers a  
354 sustainable and cost-effective approach of operation.

## 355 **Conclusion**

356 In this study, the degradation of SMX and concurrent  $\text{H}_2\text{O}_2$  production was examined in a double  
357 chamber electrochemical system equipped with BDD anode and graphite cathode separated by  
358 cation exchange membrane. The effect of various operational parameters was determined and the  
359 set of parameters at which a maximum efficiency was achieved were pH 3, 0.05 M  $\text{Na}_2\text{SO}_4$  as  
360 electrolyte, and 10 mA as applied current. Under the optimized conditions, the electrochemical  
361 setup was able to produce about 535  $\mu\text{M}$   $\text{H}_2\text{O}_2$  and 95% SMX degradation for a reaction time of  
362 180 min. The intermediate products generated during SMX electrochemical oxidation were also  
363 analyzed and a degradation pathway was proposed. It was observed that most of the transformation

364 products were formed due to the reaction with hydroxyl radicals and were less toxic compared to  
365 the parent compound. These results can act as a precursor while opting for energy-efficient and  
366 cost-effective systems in advanced wastewater treatment domain, which not only degrades the  
367 pollutant efficiently but also stores the excess energy in the form of  $H_2O_2$ , while  $H_2O_2$  can be  
368 further utilized for environmental remediation. Further work can be carried out to activate and  
369 utilize the in situ produced  $H_2O_2$  via different techniques.

### 370 **Acknowledgments**

371 This research was supported by the European Union's EU Framework Programme for Research  
372 and Innovation Horizon 2020 under Grant Agreement No 861369 (MSCA-ETN InnovEOX) and  
373 by the KU Leuven Industrial Research Council under grant number C24E/19/040  
374 (SO4ELECTRIC).

375 **References**

- 376 Ali, I., Van Eyck, K., De Laet, S., Dewil, R., 2022. Recent advances in carbonaceous catalyst  
377 design for the in situ production of H<sub>2</sub>O<sub>2</sub> via two-electron oxygen reduction. *Chemosphere*  
378 136127. <https://doi.org/10.1016/j.chemosphere.2022.136127>.
- 379 Amorim, K.P.D., Romualdo, L.L., Andrade, L.S., 2013. Electrochemical degradation of  
380 sulfamethoxazole and trimethoprim at boron-doped diamond electrode: performance, kinetics  
381 and reaction pathway. *Sep. Purif. Technol.* 120, 319–327.  
382 <https://doi.org/10.1016/j.seppur.2013.10.010>.
- 383 Barrera-Díaz, C., Canizares, P., Fernández, F.J., Natividad, R., Rodrigo, M.A., 2014.  
384 Electrochemical advanced oxidation processes: an overview of the current applications to  
385 actual industrial effluents. *J. Mex. Chem. Soc.* 58 (3), 256-275.
- 386 Calle-Vallejo, F., Martínez, J.I., García-Lastra, J.M., Abad, E., Koper, M.T.M., 2013. Oxygen  
387 reduction and evolution at single-metal active sites: comparison between functionalized  
388 graphitic materials and protoporphyrins. *Surf. Sci.* 607, 47–53.  
389 <https://doi.org/10.1016/j.susc.2012.08.005>.
- 390 Cho, S., Kim, C., Hwang, I., 2020. Electrochemical degradation of ibuprofen using an activated-  
391 carbon- based continuous- flow three-dimensional electrode reactor (3DER ). *Chemosphere*  
392 259, 127382. <https://doi.org/10.1016/j.chemosphere.2020.127382>.
- 393 Dirany, A., Sirés, I., Oturan, N., Oturan, M.A., 2010. Electrochemical abatement of the antibiotic  
394 sulfamethoxazole from water. *Chemosphere* 81 (5), 594–602.  
395 <https://doi.org/10.1016/j.chemosphere.2010.08.032>.

396 European Commission, 2020. Commission Implementing Decision (EU) 2020/1161 of 4 August  
397 2020 establishing a watch list of substances for Union-wide monitoring in the field of water  
398 policy pursuant to Directive 2008/105/EC of the European Parliament and of the Council.  
399 OJEU L257, 32–35.

400 Feng, J., Tao, Q., Lan, H., Xia, Y., Dai, Q., 2022. Electrochemical oxidation of sulfamethoxazole  
401 by nitrogen-doped carbon nanosheets composite PbO<sub>2</sub> electrode: kinetics and mechanism.  
402 *Chemosphere* 286, 131610. <https://doi.org/10.1016/j.chemosphere.2021.131610>.

403 Fu, J., Feng, L., Liu, Y., Zhang, L., Li, S., 2022. Electrochemical activation of peroxymonosulfate  
404 (PMS) by carbon cloth anode for sulfamethoxazole degradation. *Chemosphere* 287, 132094.  
405 <https://doi.org/10.1016/j.chemosphere.2021.132094>.

406 Ganiyu, S.O., Martínez-Huitle, C.A., Oturan, M.A., 2021. Electrochemical advanced oxidation  
407 processes for wastewater treatment: advances in formation and detection of reactive species  
408 and mechanisms. *Curr. Opin. Electrochem.* 27, 100678.  
409 <https://doi.org/10.1016/j.coelec.2020.100678>.

410 Garcia-Segura, S., Nienhauser, A.B., Fajardo, A.S., Bansal, R., Conrad, C.L., Fortner, J.D.,  
411 Marcos-Hernández, M., Rogers, T., Villagran, D., Wong, M.S., Westerhoff, P., 2020.  
412 Disparities between experimental and environmental conditions: Research steps toward  
413 making electrochemical water treatment a reality. *Curr. Opin. Electrochem.* 22, 9–16.  
414 <https://doi.org/10.1016/j.coelec.2020.100678>.

415 Hai, H., Xing, X., Li, S., Xia, S., Xia, J., 2020. Electrochemical oxidation of sulfamethoxazole in  
416 BDD anode system: degradation kinetics, mechanisms and toxicity evaluation. *Sci. Total*  
417 *Environ.* 738, 139909. <https://doi.org/10.1016/j.scitotenv.2020.139909>.



418 Khasawneh, O.F.S., Palaniandy, P., 2021. Occurrence and removal of pharmaceuticals in  
419 wastewater treatment plants. *Saf. Environ. Prot.* 150, 532–556.  
420 <https://doi.org/10.1016/j.psep.2021.04.045>.

421 Lan, Y., Coetsier, C., Causserand, C., Serrano, K.G., 2017. On the role of salts for the treatment  
422 of wastewaters containing pharmaceuticals by electrochemical oxidation using a boron doped  
423 diamond anode. *Electrochim. Acta* 231, 309–318.  
424 <https://doi.org/10.1016/j.electacta.2017.01.160>.

425 Lee, J.H., Kang, Y.H., Hwang, S.C., Shim, J.B., Kim, E.H., Park, S.W., 2008. Application of  
426 graphite as a cathode material for electrorefining of uranium. *Nuc. Technol.* 162 (2), 135–  
427 143. <https://doi.org/10.13182/NT08-A3940>.

428 Li, H., Quispe-Cardenas, E., Yang, S., Yin, L., Yang, Y., 2021. Electrosynthesis of >20 g/L H<sub>2</sub>O<sub>2</sub>  
429 from Air. *ACS Environ. Sci. Technol. Eng.* 2 (2), 242–250.  
430 <https://doi.org/10.1021/acsestengg.1c00366>.

431 Lin, H., Niu, J., Xu, J., Li, Y., Pan, Y., 2013. Electrochemical mineralization of sulfamethoxazole  
432 by Ti/SnO<sub>2</sub>-Sb/Ce-PbO<sub>2</sub> anode: kinetics, reaction pathways, and energy cost evolution.  
433 *Electrochim. Acta* 97, 167–174. <https://doi.org/10.1016/j.electacta.2013.03.019>.

434 Liu, Q., Li, M., Zhang, F., Yu, H., Zhang, Q., Liu, X., 2017. The removal of trimethoprim and  
435 sulfamethoxazole by a high infiltration rate artificial composite soil treatment system. *Front.*  
436 *Environ. Sci. Eng.* 11, 12. <https://doi.org/10.1007/s11783-017-0920-z>.

437 Loos, G., Scheers, T., Van Eyck, K., Van Schepdael, A., Adams, E., Van der Bruggen, B.,  
438 Cabooter, D., Dewil, R., 2018. Electrochemical oxidation of key pharmaceuticals using a  
439 boron doped diamond electrode. *Sep. Purif. Technol.* 195, 184–191.

440 <https://doi.org/10.1016/j.seppur.2017.12.009>.

441 Lu, H.F., Chen, H.F., Kao, C.L., Chao, I., Chen, H.Y., 2018. A computational study of the Fenton  
442 reaction in different pH ranges. *Phys. Chem. Chem. Phys.* 20, 22890–22901.  
443 <https://doi.org/10.1039/C8CP04381G>.

444 Marselli, B., Garcia-Gomez, J., Michaud, P.A., Rodrigo, M.A., Comninellis, C., 2003.  
445 Electrogeneration of hydroxyl radicals on boron-doped diamond electrodes. *J. Electrochem.*  
446 *Soc.* 150 (3), D79.

447 Meffe, R., de Bustamante, I., 2014. Emerging organic contaminants in surface water and  
448 groundwater: A first overview of the situation in Italy. *Sc. Total Environ.* 481, 280–295.  
449 <https://doi.org/10.1016/j.scitotenv.2014.02.053>.

450 Milh, H., Cabooter, D., Dewil, R., 2021. Role of process parameters in the degradation of  
451 sulfamethoxazole by heat-activated peroxymonosulfate oxidation: radical identification and  
452 elucidation of the degradation mechanism. *Chem. Eng. J.* 422, 130457.  
453 <https://doi.org/10.1016/j.cej.2021.130457>.

454 Milh, H., Schoenaers, B., Stesmans, A., Cabooter, D., Dewil, R., 2020. Degradation of  
455 sulfamethoxazole by heat-activated persulfate oxidation: elucidation of the degradation  
456 mechanism and influence of process parameters. *Chem. Eng. J.* 379, 122234.  
457 <https://doi.org/10.1016/j.cej.2019.122234>

458 Nabgan, W., Saeed, M., Jalil, A.A., Nabgan, B., Gambo, Y., Ali, M.W., Ikram, M., Fauzi, A.A.,  
459 Owgi, A.H.K., Hussain, I. and Thahe, A.A., 2022. A state of the art review on electrochemical  
460 technique for the remediation of pharmaceuticals containing wastewater. *Environ. Res.* 210,  
461 112975. <https://doi.org/10.1016/j.envres.2022.112975>.

462 Obata, K., Van De Krol, R., Schwarze, M., Schomäcker, R., Abdi, F.F., 2020. In situ observation  
463 of pH change during water splitting in neutral pH conditions: impact of natural convection  
464 driven by buoyancy effects. *Energy Environ. Sci.* 13 (12), 5104–5116.  
465 <https://doi.org/10.1039/D0EE01760D>.

466 Pang, Y., Xie, H., Sun, Y., Titirici, M.M., Chai, G.L., 2020. Electrochemical oxygen reduction for  
467 H<sub>2</sub>O<sub>2</sub> production: catalysts, pH effects and mechanisms. *J. Mater. Chem. A*, 8 (47), 24996–  
468 25016. <https://doi.org/10.1039/D0TA09122G>.

469 Peralta, E., Natividad, R., Roa, G., Marin, R., Romero, R., Pavon, T., 2013. A comparative study  
470 on the electrochemical production of H<sub>2</sub>O<sub>2</sub> between BDD and graphite cathodes. *Sustain.*  
471 *Environ. Res.* 23 (4), 259–266.

472 Pariente, M.I., Segura, Y., Álvarez-Torrellas, S., Casas, J.A., de Pedro, Z.M., Diaz, E., García, J.,  
473 López-Muñoz, M.J., Marugán, J., Mohedano, A.F., Molina, R., 2022. Critical review of  
474 technologies for the on-site treatment of hospital wastewater: From conventional to combined  
475 advanced processes. *J. Environ. Manage.* 320, 115769.  
476 <https://doi.org/10.1016/j.jenvman.2022.115769>.

477 Pozzo, A.D., Palma, L.D., Merli, C., Petrucci, E., 2005. An experimental comparison of a graphite  
478 electrode and a gas diffusion electrode for the cathodic production of hydrogen peroxide. *J.*  
479 *App. Electrochem.* 35 (4), 413–419. <https://doi.org/10.1007/s10800-005-0800-2>.

480 Prasannamedha, G., Kumar, P. S., 2020. A review on contamination and removal of  
481 sulfamethoxazole from aqueous solution using cleaner techniques: Present and future  
482 perspective. *J. Clea. Prod.* 250, 119553. <https://doi.org/10.1016/j.jclepro.2019.119553>.

483 Qi, H., Sun, X., Sun, Z., 2022. Cu-doped Fe<sub>2</sub>O<sub>3</sub> nanoparticles/etched graphite felt as bifunctional

484 cathode for efficient degradation of sulfamethoxazole in the heterogeneous electro-Fenton  
485 process. *Chem. Eng. J.* 427, 131695. <https://doi.org/10.1016/j.cej.2021.131695>.

486 Qiang, Z., Chang, J.H., Huang, C.P., 2002. Electrochemical generation of hydrogen peroxide from  
487 dissolved oxygen in acidic solutions. *Water Res.* 36 (1), 85–94.  
488 [https://doi.org/10.1016/S0043-1354\(01\)00235-4](https://doi.org/10.1016/S0043-1354(01)00235-4).

489 Qu, C., Liang, D.W., 2022. Novel electrochemical advanced oxidation processes with H<sub>2</sub>O<sub>2</sub>  
490 generation cathode for water treatment: A review. *J. Environ. Chem. Eng.* 107896.  
491 <https://doi.org/10.1016/j.jece.2022.107896>.

492 Radjenovic, J., Petrovic, M., 2017. Removal of sulfamethoxazole by electrochemically activated  
493 sulfate: Implications of chloride addition. *J. Hazard. Mater.* 333, 242–249.  
494 <https://doi.org/10.1016/j.jhazmat.2017.03.040>.

495 Rajab, M., Heim, C., Greco, G., Helmreich, B., Letzel, T., 2013. Removal of sulfamethoxazole  
496 from wastewater treatment plant effluents by a boron-doped diamond electrode. *Int. J.*  
497 *Environ. Pollut. and Solut.* 1 (3), 88–97. <https://doi.org/10.7726/ijeps.2013.1008>.

498 Reddy, P.M.K., Subrahmanyam, C., 2015. Catalytic plasma reactor for degradation and  
499 mineralization of pharmaceuticals and personal care products. *J. Adv. Oxid. Technol.* 18 (1),  
500 161–166. <https://doi.org/10.1515/jaots-2015-0120>.

501 Sifuna, F.W., Orata, F., Okello, V., Jemutai-Kimosop, S., 2016. Comparative studies in  
502 electrochemical degradation of sulfamethoxazole and diclofenac in water by using various  
503 electrodes and phosphate and sulfate supporting electrolytes. *J. Environ. Sci. and Health A*,  
504 51 (11), 954–961. <https://doi.org/10.1080/10934529.2016.1191814>.

505 Song, H., Yan, L., Ma, J., Jiang, J., Cai, G., Zhang, W., Zhang, Z., Zhang, J., Yang, T., 2017.  
506 Nonradical oxidation from electrochemical activation of peroxydisulfate at Ti/Pt anode:  
507 efficiency, mechanism and influencing factors. *Water Res.* 116, 182–193.  
508 <https://doi.org/10.1016/j.watres.2017.03.035>.

509 Srivastav, M., Gupta, M., Agrahari, S.K., Detwal, P., 2019. Removal of refractory organic  
510 compounds from wastewater by various advanced oxidation process-a review. *Curr. Environ.*  
511 *Eng.* 6 (1), 8–16. <https://doi.org/10.2174/2212717806666181212125216>.

512 Suzuki, N., Okazaki, A., Takagi, K., Serizawa, I., Hirami, Y., Noguchi, H., Pitchaimuthu, S.,  
513 Terashima, C., Suzuki, T., Ishida, N., Nakata, K., Katsumata, K., Kondo, T., Yuasa, M.,  
514 Fujishima, A., 2022. Complete decomposition of sulfamethoxazole during an advanced  
515 oxidation process in a simple water treatment system. *Chemosphere* 287, 132029.  
516 <https://doi.org/10.1016/j.chemosphere.2021.132029>.

517 Tian, H., Wang, Y., Pei, Y., 2020. Energy capture from thermolytic solutions and simulated  
518 sunlight coupled with hydrogen peroxide production and wastewater remediation. *Water Res.*  
519 170, 115318. <https://doi.org/10.1016/j.watres.2019.115318>.

520 Trinh, Q.D. 2011. Diffusion and Kinetic Controlled Electrochemical Reactions.  
521 <https://demonstrations.wolfram.com/DiffusionAndKineticControlledElectrochemicalReactions/>  
522 ions/ (accessed 16 August 2022).

523 Tröger, R., Ren, H., Yin, D., Postigo, C., Nguyen, P.D., Baduel, C., Golovko, O., Been, F., Joerss,  
524 H., Boleda, M.R., Polesello, S., Roncoroni, M., Taniyasu, S., Menger, F., Ahrens, L., Lai,  
525 F.Y., Wiberg, K., 2021. What’s in the water? – Target and suspect screening of contaminants  
526 of emerging concern in raw water and drinking water from Europe and Asia. *Water Res.* 198,

527 117099. <https://doi.org/10.1016/j.watres.2021.117099>.

528 Wang, J., Li, C., Rauf, M., Luo, H., Sun, X., Jiang, Y., 2021a. Gas diffusion electrodes for H<sub>2</sub>O<sub>2</sub>  
529 production and their applications for electrochemical degradation of organic pollutants in  
530 water: A review. *Sci. Total Environ.* 759, 143459.  
531 <https://doi.org/10.1016/j.scitotenv.2020.143459>.

532 Wang, N., Ma, S., Zuo, P., Duan, J., Hou, B., 2021b. Recent progress of electrochemical  
533 production of hydrogen peroxide by two-electron oxygen reduction reaction. *Adv. Sci.* 8 (15),  
534 2100076. <https://doi.org/10.1002/advs.202100076>.

535 Wang, Y., Zhou, C., Wu, J., Niu, J., 2020. Insights into the electrochemical degradation of  
536 sulfamethoxazole and its metabolite by Ti/SnO<sub>2</sub>-Sb/Er-PbO<sub>2</sub> anode. *Chin. Chem. Lett.* 31  
537 (10), 2673–2677. <https://doi.org/10.1016/j.ccllet.2020.03.073>.

538 Xue, Y., Wang, Y., Pan, Z., Sayama, K., 2021. Electrochemical and photoelectrochemical water  
539 oxidation for hydrogen peroxide production. *Angewandte Chemie International Edition*, 60  
540 (19), 10469–10480. <https://doi.org/10.1002/anie.202011215>.

541 Yang, Y., Lu, X., Jiang, J., Ma, J., Liu, G., Cao, Y., Liu, W., Li, J., Pang, S., Kong, X., Luo, C.,  
542 2017. Degradation of sulfamethoxazole by UV, UV/H<sub>2</sub>O<sub>2</sub> and UV/persulfate (PDS):  
543 formation of oxidation products and effect of bicarbonate. *Water Res.* 118, 196–207.  
544 <https://doi.org/10.1016/j.watres.2017.03.054>.

545 Zhang, B., Xu, W., Lu, Z., Sun, J., 2020. Recent progress on carbonaceous material engineering  
546 for electrochemical hydrogen peroxide generation. *Trans. Tianjin Univ.* 26 (3), 188– 96.  
547 <https://doi.org/10.1007/s12209-020-00240-0>.

548 Zhu, X., Tong, M., Shi, S., Zhao, H., Ni, J., 2008. Essential explanation of the strong mineralization  
549 performance of boron-doped diamond electrodes. *Environ. Sci. Technol.* 42 (13), 4914–4920.  
550 <https://doi.org/10.1021/es800298p>.